

A high Neel temperature 5d oxide: NaOsO₃

S. Middey,^{1,*} Saikat Debnath,² Priya Mahadevan,^{2,†} and D. D. Sarma^{3,4}

¹Centre for Advanced Materials, Indian Association for the Cultivation of Science, Jadavpur, Kolkata-700032, India

²S. N. Bose National Centre for Basic Sciences,
JD-Block, Sector III, Salt Lake, Kolkata-700098, India

³Solid State and Structural Chemistry Unit, Indian Institute of Science, Bangalore-560012, India

⁴Council of Scientific and Industrial Research - Network of Institutes for Solar Energy (CSIR-NISE), New Delhi, India

The origin of a high Neel temperature in a 5d oxide, NaOsO₃, has been analyzed within the mean-field limit of a multiband Hubbard model and compared with the analogous 4d oxide, SrTcO₃. Our analysis shows that there are a lot of similarities in both these oxides on the dependence of the effective exchange interaction strength (J_0) on the electron-electron interaction strength (U). However, the relevant value of U in each system puts them in different portions of the parameter space. Although the Neel temperature for NaOsO₃ is less than that for SrTcO₃, our results suggest that there could be examples among other 5d oxides which have a higher Neel temperature. We have also examined the stability of the G-type antiferromagnetic state found in NaOsO₃ as a function of electron doping within GGA+U calculations and find a robust G-type antiferromagnetic metallic state stabilized. The most surprising aspect of the doped results is the rigid band-like evolution of the electronic structure which indicates that the magnetism in NaOsO₃ is not driven by fermi surface nesting.

PACS number(s): 75.10.-b, 75.47.Lx, 71.30.+h

I. INTRODUCTION

Metal-insulator transitions in strongly correlated systems, especially transition metal oxides still continue to be an important topic of research as new and unusual examples emerge¹. The transitions in these systems have been understood within the Hubbard model² and arise from a competition between localizing effects controlled by the onsite Coulomb interaction strength U and electron delocalization effects governed by the bandwidth, W . Within the Hubbard model, the system is insulating when U/W is greater than 1, and a change of this ratio (across 1) by doping, external pressure etc. are routes by which one can induce a metal-insulator transition. While a lot of examples exist among the 3d oxides, there are very few insulating members among the 4d and 5d perovskite oxides. The larger spatial extent of the 4d and the 5d orbitals results in a larger bandwidth, and the additional screening effects present in these larger bandwidth oxides are expected to result in a reduced U . Consequently, the smaller U/W ratio, expected to be less than 1, explains the metallic ground states observed in most cases. The few insulating examples that one finds there, require some other mechanism than the Mott transition to explain the ground state character. Recently, Shi *et al.* found a metal-insulator transition in NaOsO₃ at 410 K³, which has been observed as arising from the onset of antiferromagnetic order, thus the system is a perfect illustration of Slater insulator⁴. Very recent neutron and X-ray scattering studies and optical spectroscopy further confirm the picture of a Slater transition in this compound^{5,6}. As any long range magnetic order requires correlated electrons, it is rather a surprise, that the magnetic transition temperature of NaOsO₃ is so high (410

K). Local magnetic moments are usually very small in 5d oxides as a result of the wide bands, so large ordering temperatures are quite unexpected.

The basic electronic structure of NaOsO₃ has been calculated before^{3,7,8}, though the key question of why one has such a high ordering temperature in a 5d oxide is still not well understood. Du *et al.*⁷ recently showed that in spite of Os being a 5d transition metal atom, spin-orbit interactions seem to have a weak effect on the band structure in NaOsO₃. The states near the fermi level seem to be strongly itinerant with a strong admixture of Os d and O p states suggesting that the appropriate picture of magnetism seems to be an itinerant one. Further, they conclude by saying that the magnetic ordering as well as coulomb interactions play a role in making NaOsO₃ insulating. The nature of magnetism and the origin of the insulating state has been raised by Jung *et al.*⁸. Considering a cubic ideal perovskite structure for NaOsO₃, they find that a small rotation of the OsO₆ octahedra is able to drive NaOsO₃ insulating as well as stabilize G-type antiferromagnetic ordering. Consequently, this should be characterized by a spin spiral vector $q=0$ in contrast to a fermi surface nesting or hot spot driven magnetic transitions which are characterised by a non-zero nesting vector. This makes the nature of the observed magnetic transition in NaOsO₃ even more puzzling, though Slater made the observation in his seminal paper⁴ that the up and down spin electrons see different potentials, and by that definition, even a transition characterized by a $q=0$ spin spiral vector should fit in as a Slater transition.

In the present work, we have calculated the electronic and magnetic structure of NaOsO₃ within GGA based ab-initio electronic structure calculations. Both the G-AFM ground state as well as its insulating nature are captured within these calculations. In order to understand the origin of the magnetic state, we perform further analysis within a multiband Hubbard model where

the tight binding part is determined from a fitting of the ab-initio band structure. At a U of just 0.8 eV, one is able to stabilize an insulating G-AFM state as the ground state. This scale of U is far less than the bandwidth of ~ 3 eV, suggesting that the scale of U is irrelevant, and we have been able to capture the Slater insulator limit within our calculations. Varying U and the charge transfer energy, one finds a wide range of parameter space for which the G type AFM solution is the ground state indicating the robustness of the magnetism. The origin of the magnetism can be traced back to the strong bonding-antibonding splitting arising from the interaction between nearest neighbor Os atoms. As the t_{2g} levels are half-filled here, this energy gain is possible only for an antiferromagnetic configuration, while in the fully spin polarised limit the ferromagnetic configuration has no energy gain associated with it. Surprisingly, the small intraatomic exchange splitting and the large bandwidth aid to stabilize the magnetic state more as we pointed out in an earlier work⁹, though the naive expectation would be that it destabilizes magnetism. This picture is further strengthened by our studies carried out as a function of doping. While the filling should be important in a model where magnetism is nesting-driven, in the present case we find that the G-type antiferromagnetism is robust even away from half-filling, though the ground state now becomes metallic. Examining the exchange interaction strengths in the doped systems, we find an additive nature of the magnetic interactions emerges, with the partial filling of the Os $d t_{2g}$ minority spin levels contributing a ferromagnetic component. This route is also suggestive of a clean route to obtain an antiferromagnetic metal as there is no strong electron-phonon coupling physics to be found here.

The mechanism for magnetism proposed here for NaOsO₃ is similar what we had shown earlier⁹ for a wide variety of compounds which include SrTcO₃¹⁰, CaTcO₃¹¹ etc. though NaOsO₃ has much smaller T_N (410 K) compared to SrTcO₃ (1023 K). This difference has been explained in the present work by a study of the variation of the effective exchange interaction strengths J_0 as a function of U . SrTcO₃ lies at the peak of the curve, while NaOsO₃ lies in the rising part. This suggests that one may be able to find a different 5d oxide which could have a T_c higher than SrTcO₃.

II. METHODOLOGY

The electronic and magnetic structure of NaOsO₃ has been calculated within a plane wave pseudopotential implementation of density functional theory using PAW potentials¹² as implemented in VASP¹³. In addition to the GGA form for the exchange correlation functional, we have also considered electron-electron interactions in the d states of Os by considering a U on Os in the Dudarev implementation¹⁴ of the GGA + U scheme. Different magnetic configurations¹⁵ were examined for dif-

ferent values of U . In our calculations we used a k-mesh of $6 \times 6 \times 6$ k-points and a cut off energy of 400 eV for the plane wave basis states. In these calculations, the lattice constants were kept fixed at the experimental values³, while the internal coordinates were optimized to minimize the total energy. We have used a sphere of radius 1.44 Å about Os, 1.66 Å about Na and 0.73 Å about O for the calculation of the partial density of states as well the magnetic moment. In order to understand the origin of the observed magnetic stability and its dependence on microscopic parameters U , charge transfer energy (Δ), we carried out additional analysis in terms of a multi-band Hubbard-like Hamiltonian given by equation 1.

$$H = \sum_{i,l,\sigma} \epsilon_p p_{il\sigma}^\dagger p_{il\sigma} + \sum_{i,l,\sigma} \epsilon_d d_{il\sigma}^\dagger d_{il\sigma} + \sum_{i,j,l_1,l_2,\sigma} (t_{i,j,pp}^{l_1 l_2} p_{il_1\sigma}^\dagger p_{jl_2\sigma} + h.c.) + \sum_{i,j,l_1,l_2,\sigma} (t_{i,j,pd}^{l_1 l_2} d_{il_1\sigma}^\dagger p_{jl_2\sigma} + h.c.) + \sum_{\alpha\beta\gamma\delta,\sigma_1\sigma_2\sigma_3\sigma_4} U_{dd}^{\alpha\beta\gamma\delta} d_{\alpha\sigma_1}^\dagger d_{\beta\sigma_2}^\dagger d_{\gamma\sigma_3} d_{\delta\sigma_4} \quad (1)$$

where $d_{il\sigma}^\dagger$ ($d_{il\sigma}$) creates (annihilates) an electron with spin σ in the l^{th} d -orbital on Os in the i^{th} unit cell, $p_{im\sigma}^\dagger$ ($p_{im\sigma}$) creates (annihilates) an electron with spin σ

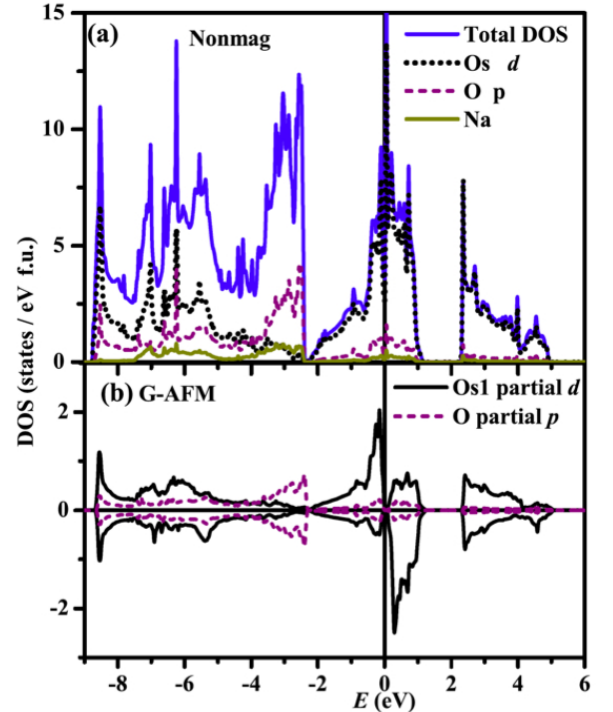


FIG. 1. (color online) Density of states of NaOsO₃ obtained from GGA calculation ($U = 0$) (a) The total as well as partial density of states for nonmagnetic configuration. (b) The up (upper panel) and the down spin (lower panel) Os d projected partial density of states for G-AFM magnetic structure. The zero of energy corresponds to the Fermi energy.

in the m^{th} p -orbital on oxygen atom in the i^{th} unit cell. The details about solving this Hamiltonian can be found in Ref. ⁹. The total energies for different magnetic configurations were mapped onto a Heisenberg model ($-\frac{1}{2} \sum J_{ij} s_i \cdot s_j$) with first neighbor (J_1) as well as second neighbor (J_2) exchange interaction strengths. For the structures considered an effective exchange interaction strength J_0 given by $6J_1 + 12J_2$ was determined in each case, as it could be related to the mean field T_N .

The robustness of the results to electron doping has been examined by considering the 20 atom supercell of NaOsO_3 and replacing one or two Na atoms by Mg. This corresponds to an average occupancy of 3.25 or 3.5 at the Os site. Various magnetic configurations have been considered and we discuss the stability of the G-AFM state as a function of doping. Additionally, we have considered various non-collinear magnetic configurations in the vicinity of the G-AFM state and determined their energies to see if any spin spiral magnetic solution had lower energy. Spin-orbit interactions are large in $5d$ oxides and so we have calculated the stability of the G-AFM state including spin-orbit interactions to probe the role of spin-orbit interactions.

III. RESULTS AND DISCUSSIONS

The magnetic stabilization energies for different magnetic configurations calculated from our *ab-initio* calculations are given in Table I. In each case the energies are referenced to the nonmagnetic configuration. For the calculations in which we have $U = 0$, we find that all

TABLE I. Stabilization energy (meV/f.u.) with respect to the nonmagnetic state from GGA+U calculations.

U(eV)	Ferro	A-AFM	C-AFM	G-AFM
0	nonmag	nonmag	nonmag	-20
1	-7	-11	-50	-127
2	-111	-132	-225	-314
3	-295	-415	-521	-587

the magnetic configurations except the G-AFM configuration converge to nonmagnetic solutions. The stability of the G-AFM state is found to be large with respect to the nonmagnetic configuration. The robustness of the G-AFM configuration vis-a-vis other magnetic configurations has been observed and discussed earlier in the context of SrTeO_3 ⁹. This has been traced back to the large superexchange energy gain arising between nearest neighbor antiferromagnetic spins for a half-filling of the t_{2g} orbitals on Os. As the G-type antiferromagnetic configuration has all nearest neighbor spins antiferromagnetically coupled, this energy gain from the superexchange mechanism is the largest, and hence it is stabilized the most. When U is increased to 1 eV, one finds an increase in the stabilization energy for the G-AFM state with respect to the closely competing C-type antiferromagnetic configuration, which then begins to decrease as U is increased further. The origin for this is clearer from the model Hamiltonian calculations discussed later in the paper.

The total and partial density of states (DOS) for the nonmagnetic solution is plotted in Fig.1(a). The nonmagnetic solution is metallic, with the Fermi energy E_F lying in the middle of the t_{2g} antibonding states. The large width (greater than 3 eV) of the t_{2g} antibonding states and the significant admixture of Os d and O p states appear due to the larger spatial extent of the $5d$ orbitals. Na acts as a perfect electron donor as suggested by the absence of significant Na partial density states (PDOS) near E_F . The up and down spin Os d partial density of states for the G-AFM configuration is shown in Fig. 1(b). The G-AFM magnetic ordering modifies the DOS as shown in Fig. 1(b) by opening up a small gap at E_F . The magnetic moment on Os is found to be just $0.90 \mu_B$, close to the experimentally observed moment of $1 \mu_B$ ⁵, but much smaller than the anticipated value of $3 \mu_B$ which is expected for a d^3 configuration. The reduction in magnetic moment in this class of materials has sometimes been referred to as arising from spin fluctuation effects. The fact that we can capture this reduction in a mean field picture, that there is some other mechanism at play. The reason for this is evident from the density of states which indicates a significant Os minority spin contribution in the density of states. Using a $U = 1$ eV on the Os d states, we found that all the collinear magnetic configurations could be converged to magnetic solutions. Considering the G-type AFM solu-

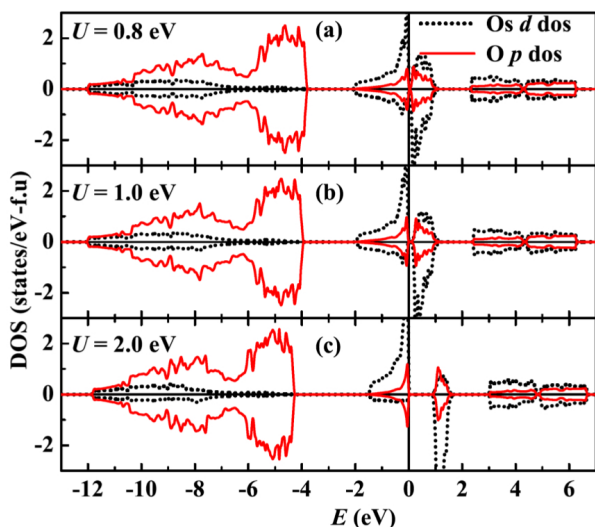


FIG. 2. (color online) The Up (upper panel) and down spin (lower panel) projected Os d and O p partial density of states for G-AFM spin configuration for $\Delta=2$ eV, $J_h=0.1$ eV as a function of U from mean-field multiband Hubbard calculations for NaOsO_3 . The zero of energy corresponds to the Fermi energy.

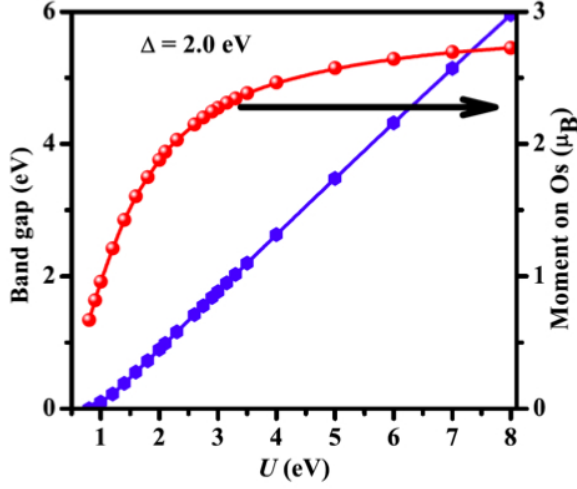


FIG. 3. (color online) The variation of the band gap (left axis) and the magnitude of magnetic moment of each Os atom (right axis) as a function of U are plotted for $\Delta = 2.0$ eV.

tion, one finds that the band gap for the is found to be 0.3 eV and the magnetic moment on Os is found to be $1.3 \mu_B$.

To understand the origin of magnetic ordering and the simultaneous metal-insulator transition, we set up a multiband Hubbard-like model for NaOsO_3 with a U on the Os d states and calculated the electronic and magnetic ground states as a function of U as well as the charge transfer energy Δ . The hopping matrix elements were parameterized in terms of the Slater Koster parameters $pd\sigma$, $pd\pi$, $sd\sigma$, $pp\sigma$ and $pp\pi$ ^{16,17}. A least squared error minimization procedure was used to estimate the best set of parameters entering the tight-binding part of the Hamiltonian that best fit the *ab-initio* band structure¹⁸. The bands with primarily Os d character as well as the O p nonbonding states were included in the fitting. The best-fit parameters were found to be $sd\sigma = -3.65$ eV, $pd\sigma = -3.75$ eV, $pd\pi = 1.80$ eV, $pp\sigma = 0.7$ eV and $pp\pi = -0.15$ eV and $\epsilon_d - \epsilon_p = 0.8$ eV. The larger values of $pd\sigma$, $pd\pi$ compared to SrTcO_3 , SrMnO_3 ⁹ are expected for a $5d$ oxide and are due to the more extended nature of the $5d$ orbitals.

The multiband Hubbard Hamiltonian for NaOsO_3 has been solved for several values of U using a mean-field decoupling scheme for the four fermion term. We used a small value of 0.1 eV for the intraatomic Hund's exchange interaction strength and initially kept $\Delta (= \epsilon_d - \epsilon_p + 3U)$ fixed at 2 eV. Again as observed in the case of the *ab-initio* calculations, here also we found that the G-type antiferromagnetic solution converged easily for even a small value of U of 0.8 eV, while other magnetic configurations considered did not converge to a magnetic ground state. Further, the G-AFM configuration remained to be the ground state even as U was increased. In our calculations we have varied U upto 8 eV. The Os d and O p partial density of states are plotted for the G-AFM con-

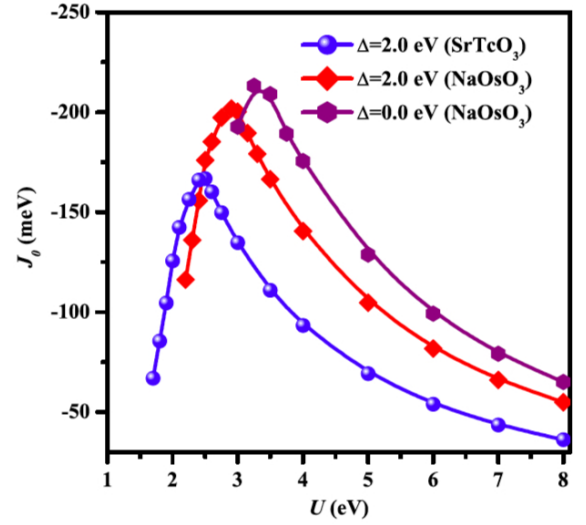


FIG. 4. (color online) Variation of effective exchange interaction strength (J_0) with U for $J_h = 0.1$ eV from mean field multiband calculations for $\Delta=2$ and 0 eV respectively. The hopping interaction strengths for the tight-binding part of the Hamiltonian are taken for the system shown in parentheses.

figuration in Fig. 2 for several values of U . A bandgap is found to barely open up at a value of $U = 0.8$ eV and this gradually increases as the value of U is increased to 2 eV. Plotting the variation of the band gap (E_g) one finds an almost linear increase (Fig. 3). At lower values of U one finds a significant contribution to the Os d occupied partial density of states from the minority spin channel. This explains the strong reduction that one finds in the magnetic moment from the value of $3 \mu_B$ expected for a d^3 electronic configuration. As the U value is increased, the individual moment on each Os site increases and goes near saturation at larger U values (Fig. 3). For the ferromagnetic case as well as the other antiferromagnetic configurations where some neighboring spins are aligned ferromagnetically, the metal-insulator transition takes place at a larger value of U .

The next question we went on to address was whether the fact that SrTcO_3 had a higher T_N than NaOsO_3 was indicative of a general trend that $4d$ transition metal oxides would have a higher ordering temperature than $5d$ transition metal oxides. To examine this we have calculated J_0 as a function of U for the two systems. This is plotted in Fig. 4 for $J_h=0.1$ eV and $\Delta=2$ eV. For small values of U , some of the magnetic configurations did not converge to magnetic solutions. Consequently J_0 could not be estimated there. One aspect that is immediately apparent from Fig. 4 is that the variation of J_0 is similar in both systems. The differences arise from the larger $p-d$ hopping strength that we have for NaOsO_3 as compared with SrTcO_3 . The peak of J_0 appears at $U = 2.5$ eV and 2.9 eV for SrTcO_3 and NaOsO_3 respectively. The value of J_0 at the peak is also much higher for NaOsO_3 than for SrTcO_3 . Now although we refer to the curve as rep-

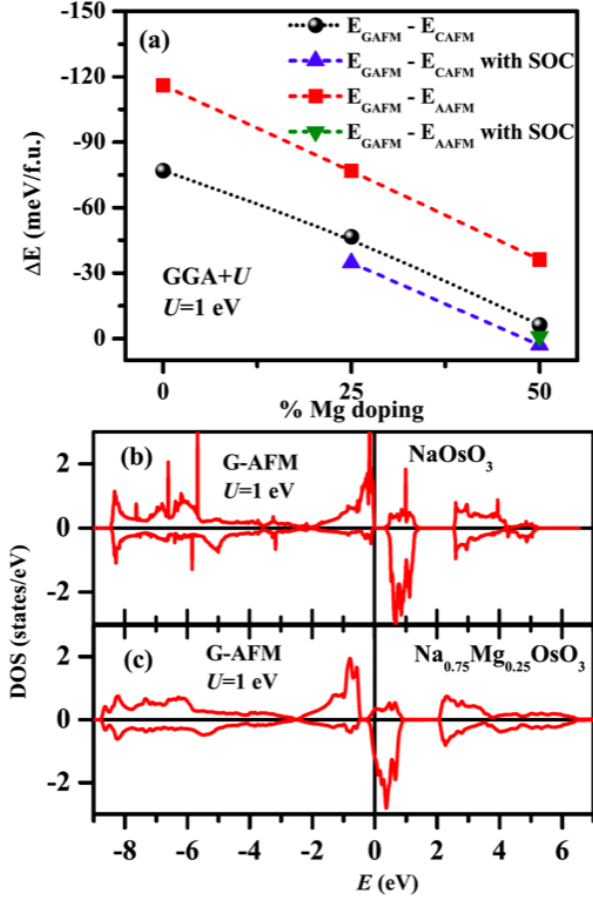


FIG. 5. (color online) (a) Variation of magnetic stabilization energy of G-AFM configuration with Mg doping ($U = 1$ eV) from GGA+ U calculations. Up (upper panel) and down spin (lower panel) Os d projected partial density of states for (b) NaOsO_3 and (c) $\text{Na}_{0.75}\text{Mg}_{0.25}\text{OsO}_3$ at $U = 1$ eV in the G-AFM configuration.

representing variations for NaOsO_3 and SrTcO_3 , these systems represent just one point on the curve, characterised by the relevant U for the system. The electron correlation strength in NaOsO_3 is expected to be much smaller than the U value where J_0 has a peak. On the other hand, SrTcO_3 is located near the peak in J_0 . This explains why NaOsO_3 has a smaller T_N . However, one could have another $5d$ oxide which could have a much higher T_N than SrTcO_3 . To emphasize this point, we have varied Δ to 0 eV and plotted the variation of J_0 in NaOsO_3 . A smaller Δ is expected to result in an increased superexchange interaction strength between nearest neighbor sites. This results in an increased J_0 compared to the larger Δ solutions for the same value of U . The peak in J_0 is also found to shift to a larger U .

Fermi surface nesting of a bipartite lattice¹⁹ is generally used to explain the insulating ground state that emerges for the G-AFM magnetic structure. A small doping should take one away from the point where a robust G-AFM magnetic solution is found and so one does

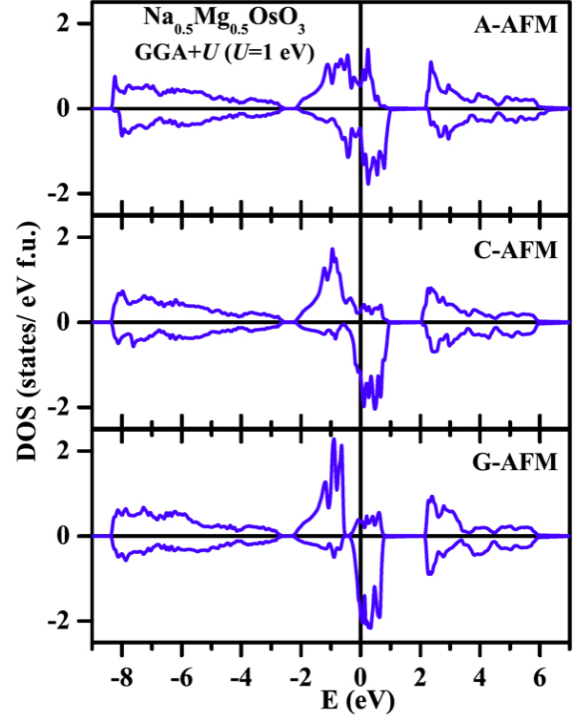


FIG. 6. (color online) Up (upper panel) and down spin (lower panel) Os d projected partial density of states for $\text{Na}_{0.50}\text{Mg}_{0.50}\text{OsO}_3$ in various magnetic configurations from GGA+ U calculations. The zero of energy represents the fermi energy.

not expect any magnetic solution to be stable. In order to examine this aspect, monovalent Na of NaOsO_3 has been replaced partially by divalent Mg and the energy of various magnetic configurations have been calculated within *ab-initio* GGA+ U calculations. The lattice constants were fixed at the experimental value of NaOsO_3 , while the internal coordinates were optimized. The stabilization energy of the lowest energy configuration (G-AFM) has been plotted in Fig. 5(a) with respect to other antiferromagnetic configurations (C-AFM, A-AFM) as a function of Mg doping. Interestingly, we find an almost linear variation of the stabilization energies with doping. With an increase in Mg doping i.e. electron doping, the energy difference decreases and for 50% doping case, the C-type and G-type antiferromagnetic configurations are almost degenerate. Spin-orbit interactions are believed to be sizable in $5d$ oxides and could be of the same strength as the intra-atomic exchange interaction strength^{20,21}. Consequently, we went on to examine if including spin-orbit interactions modified the conclusions we had in the absence of including spin-orbit interactions. A similar trend in the magnetic stabilization energies was found even in the presence of spin-orbit interactions with the G-AFM spin configuration still found to be the ground state for the 25% doped case.

The up and down spin Os d partial density of states within the *ab-initio* calculations for $U=1$ are plotted in

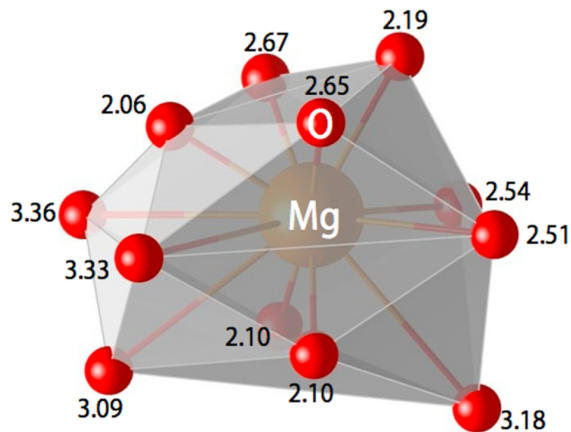


FIG. 7. (color online) Distortion in Mg-O bond lengths for 3.125% Mg doped case.

Figs. 5(b) and (c) for NaOsO_3 as well as the 25% doped case in the G-AFM magnetic structure. Surprisingly, one finds an almost rigid band evolution of the density of states in the doped system. A similar magnitude of the energy gap between the majority spin and minority spin t_{2g} states is found with all other aspects of the electronic structure remain the similar. The Mg doping has now resulted in a shift of the fermi level into the minority spin t_{2g} states and we have a rare occurrence of an antiferromagnetic metallic state.

It is also interesting to note that while the t_{2g} states show a large exchange splitting, the e_g states which are at higher energies show hardly any exchange splitting. This is because the intra-atomic exchange splitting in these systems is small, and whatever exchange splitting one finds for the t_{2g} states, emerges from the superexchange interactions, primarily from nearest neighbor Os atoms. This effect is even more evident in Fig. 6 where we have plotted the up and down spin Os d partial density of states for different magnetic configurations for 50% Mg doped NaOsO_3 . The number of antiferromagnetic neighbors increases from A-AFM configuration to the C-AFM configuration to the G-AFM configuration. The exchange splitting is also found to increase with the number of antiferromagnetic neighbors contributing to the superexchange pathways. While there is no band gap between the majority spin and the minority spin t_{2g} states for both A and C-AFM configurations, a small band gap exists for the G-AFM magnetic structure, again emerging for the same reasons.

In order to examine the stability of this antiferromagnetic state to the formation of polarons, we have constructed a 160 atom unit cell of NaOsO_3 and in that cell we have replaced one Na atom with Mg atom. We find that there are strong lattice relaxations of the oxygen atoms which form the first shell of neighbours around Mg. We show that the first shell of Mg-O atoms. Significant distortions are found with the shortest bond length equal

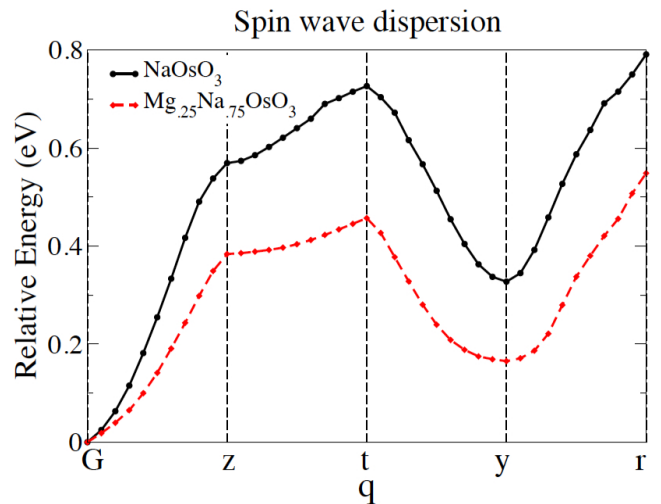


FIG. 8. (color online) Spin wave dispersion along different symmetry directions for NaOsO_3 and 25% Mg doped case. The zero of energy corresponds to energy of G-AFM state for both cases.

to 2.06 Å as shown in Fig. 7. However there is a very small effect on the Os-O bond lengths. Hence no strong electron-phonon physics are operative here. Hence doping electrons into a 5d oxide does not have the problems one encounter with 3d oxides such as the manganites²² where polaron formation has been reported. These systems are suggestive of a facile route to a G-type antiferromagnetic metallic solution.

In Fig. 5(a) we have reported the magnetic stabilization energies for few collinear configurations. The immediate question which arises is whether we have probed enough magnetic configurations as the doped systems could have spin spiral configurations being favoured. We have therefore considered excitations about the G-type antiferromagnetic configuration and examined various spin spiral configurations characterized by the spin spiral vector q as plotted in Fig. 8. The G point which has the lowest energy corresponds to the G-type antiferromagnetic solution. This is metallic for the 25% Mg doped NaOsO_3 while it is insulating for the undoped case. Both these solutions establish that electron doping indeed stabilizes G-type antiferromagnetic metallic state in this system.

IV. CONCLUSIONS

We have studied the origin of a high Neel temperature in 5d oxide NaOsO_3 within the mean-field limit of a multiband Hubbard model and compared that with 4d oxides SrTcO_3 . Both these compounds show very similar trends in the variation of the exchange interaction strengths. The relevant strength of J_0 for NaOsO_3 places it in a region where J_0 increases with an increase in U whereas SrTcO_3 is located near the peak in J_0 . Examining

ing the relevant parameter space for $5d$ oxides, our analysis also suggests that a higher T_N is possible in a $5d$ oxide by a suitable tuning of the parameters. Additionally, we have examined the stability of the G-type antiferromagnetic state on electron doping. Not only do we obtain a rigid band-like evolution of the electronic structure on doping, but also we find that the G-type antiferromagnetism remains robust even when the system becomes metallic. These systems throw up a rare occurrence of an antiferromagnetic metal. Important insights into the

nature of magnetism of the parent compound can be inferred from the doping dependent studies.

V. ACKNOWLEDGEMENT

SM and SD thank CSIR, India for fellowship. DDS and PM thank the Department of Science and Technology, India.

-
- * Present address: Department of Physics, University of Arkansas, Fayetteville, Arkansas 72701, USA
- † Corresponding author: priya.mahadevan@gmail.com
- ¹ M. Imada, A. Fujimori, and Y. Tokura, *Rev. Mod. Phys.* **70**, 1039 (1998).
- ² J. Hubbard, *Proc. R. Soc. A* **276**, 238 (1963).
- ³ Y. G. Shi, Y. F. Guo, S. Yu, M. Arai, A. A. Belik, A. Sato, K. Yamaura, E. Takayama-Muromachi, H. F. Tian, H. X. Yang, J. Q. Li, T. Varga, J. F. Mitchell, and S. Okamoto, *Phys. Rev. B* **80**, 161104 (2009).
- ⁴ J. C. Slater, *Phys. Rev.* **82**, 538 (1951).
- ⁵ S. Calder, V. O. Garlea, D. F. McMorrow, M. D. Lumsden, M. B. Stone, J. C. Lang, J.-W. Kim, J. A. Schlueter, Y. G. Shi, K. Yamaura, Y. S. Sun, Y. Tsujimoto, and A. D. Christianson, *Phys. Rev. Lett.* **108**, 257209 (2012).
- ⁶ I. Lo Vecchio, A. Perucchi, P. Di Pietro, O. Limaj, U. Schade, Y. Sun, M. Arai, K. Yamaura, and S. Lupi, *Sci. Rep.* **3**, 2990 (2013).
- ⁷ Y. Du, X. Wan, L. Sheng, J. Dong, and S. Y. Savrasov, *Phys. Rev. B* **85**, 174424 (2012).
- ⁸ M.-C. Jung, Y.-J. Song, K.-W. Lee, and W. E. Pickett, *Phys. Rev. B* **87**, 115119 (2013).
- ⁹ S. Middey, A. K. Nandy, S. K. Pandey, P. Mahadevan and D.D. Sarma, *Phys. Rev. B* **86**, 104406 (2012).
- ¹⁰ E. E. Rodriguez, F. Poineau, A. Llobet, B. J. Kennedy, M. Avdeev, G. J. Thorogood, M. L. Carter, R. Seshadri, D. J. Singh, and A. K. Cheetham, *Phys. Rev. Lett.* **106**, 067201 (2011).
- ¹¹ M. Avdeev, G. J. Thorogood, M. L. Carter, B. J. Kennedy, J. Ting, D. J. Singh, and K. S. Wallwork, *J. Am. Chem. Soc.* **133**, 1654 (2011).
- ¹² P. E. Blöchl, *Phys. Rev. B* **50**, 17953 (1994); G. Kresse and D. Joubert, *ibid.* **59**, 1758 (1999).
- ¹³ G. Kresse, and J. Furthmüller, *Phys. Rev. B* **54**, 11169 (1996); *Comput. Mater. Sci.* **6**, 15 (1996).
- ¹⁴ S. L. Dudarev, G. A. Botton, S. Y. Savrasov, C. J. Humphreys, and A. P. Sutton, *Phys. Rev. B* **57**, 1505 (1998).
- ¹⁵ The spin arrangements for different antiferromagnetic configurations can be found in Ref. ⁹.
- ¹⁶ J. C. Slater, and G. F. Koster, *Phys. Rev.* **94**, 1498 (1954).
- ¹⁷ L. F. Mattheiss, *Phys. Rev. B* **2**, 3918 (1970).
- ¹⁸ P. Mahadevan, N. Shanthi, and D. D. Sarma, *Phys. Rev. B* **54**, 11199 (1996).
- ¹⁹ J. E. Hirsch, *Phys. Rev. B* **31**, 4403 (1985).
- ²⁰ D. Haskel, G. Fabbri, Mikhail Zhernenkov, P. P. Kong, C. Q. Jin, G. Cao, and M. van Veenendaal, *Phys. Rev. Lett.* **109**, 027204 (2012).
- ²¹ B. J. Kim, Hosub Jin, S. J. Moon, J.-Y. Kim, B.-G. Park, C. S. Leem, Jaeyun Yu, T. W. Noh, C. Kim, S.-J. Oh, J.-H. Park, V. Durairaj, G. Cao, and E. Rotenberg, *Phys. Rev. Lett.* **101**, 076402 (2008).
- ²² M. B. Salamon, and M. Jaime, *Rev. Mod. Phys.* **73**, 583 (2001).